Journal of Power Sources 232 (2013) 332–337

Contents lists available at SciVerse ScienceDirect

Journal of Power Sources

journal homepage: www.elsevier.com/locate/jpowsour

Short communication

$La_{0.8}Sr_{1.2}CoO_{4+\delta}$–CGO composite as cathode on $La_{0.9}Sr_{0.1}Ga_{0.8}Mg_{0.2}O_{3-\delta}$ electrolyte for intermediate temperature solid oxide fuel cells

Jun Zhou, Gang Chen*, Kai Wu, Yonghong Cheng

State Key Laboratory of Electrical Insulation and Power Equipment, Xi'an Jiaotong University, Xi'an 710049, People's Republic of China

HIGHLIGHTS

- LSCO4 oxide is chemically compatible with CGO and LSGM electrolyte at 1100 °C.
- A low electrode polarization resistance of 0.21 Ω cm^2 is achieved at 750 °C.
- The low ASR exhibits high electrochemical activity at intermediate temperature range.
- The single cell shows a maximum cell power density of 515 mW cm^{-2} at 750 °C.
- The LSCO4–CGO composite oxides are one of promising cathode candidates for IT-SOFCs.

GRAPHICAL ABSTRACT

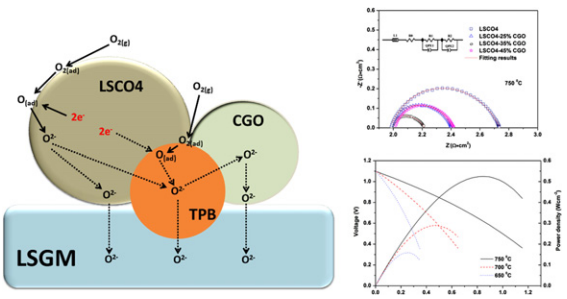

ARTICLE INFO

Article history:
Received 27 August 2012
Received in revised form
21 November 2012
Accepted 27 November 2012
Available online 22 December 2012

Keywords:
Solid oxide fuel cells
Cathode materials
Mixed ionic–electronic conductor
Electrochemical property

ABSTRACT

$La_{0.8}Sr_{1.2}CoO_{4+\delta}$ (LSCO4) material with K_2NiF_4-type structure has been synthesized via a citric–nitrate process and characterized. Composite materials $La_{0.8}Sr_{1.2}CoO_{4+\delta}$-$Ce_{0.9}Gd_{0.1}O_{2-\delta}$ (CGO) (LSCO4–CGO) have been prepared and evaluated as cathode for intermediate temperature SOFC (IT-SOFC) based on $La_{0.9}Sr_{0.1}Ga_{0.8}Mg_{0.2}O_{3-\delta}$ (LSGM) electrolytes. LSCO4 oxide is chemically compatible with CGO and LSGM electrolyte at temperature up to 1000 °C. Compared with the pure LSCO4, the optimum composition of LSCO4–35 wt % CGO exhibits better electrochemical activity for oxygen reduction. Also, for LSCO4–35 wt % CGO electrode, SEM results suggest that better microstructure is obtained and the electrode forms good contact with the electrolyte after sintering at 1000 °C for 2 h. At 750 °C, the polarization resistance of the LSCO4–35 wt % CGO composite cathode is about 0.21 Ω cm^2 in air. A cell with a 1.2 mm thick LSGM electrolyte, NiO as anode, and LSCO4-35 wt % CGO as cathode displays a maximum power density of 515 mW cm^{-2} at 750 °C. These results indicate that LSCO4–CGO composite materials are promising cathode candidates for intermediate-temperature solid oxide fuel cells with LSGM electrolyte.

1. Introduction

The solid oxide fuel cell (SOFC) is one of the most exciting systems for next power generation due to its potential fuel flexibility and very high efficiency. Nowadays, one of the most important research aims is to develop intermediate-temperature solid oxide fuel cells (IT-SOFCs, operating temperature: 600–800 °C). This would have several benefits including a longer device operating life and reduction in production costs. Reducing the operating temperature with sufficient power output and durability appears to be the challenge of IT-SOFCs [1]. Especially, one of the major problems is the high polarization resistance of the cathode at lower

* Corresponding author. Tel./fax: +86 29 82668493.
E-mail addresses: stonezhj@stu.xjtu.edu.cn, jz27@st-andrews.ac.uk (J. Zhou), chainway@mail.xjtu.edu.cn (G. Chen).

0378-7753/$ – see front matter © 2012 Elsevier B.V. All rights reserved.
http://dx.doi.org/10.1016/j.jpowsour.2012.11.110

operating temperature [2]. Thus, it is critical to develop new cathode materials with proper electrochemical performance at low operation temperature. Generally, the cathode should posses many properties including high-catalytic activity for oxygen reduction, high-electrical conductivity, thermal stability, and compatibility with other cell components. Mixed ionic and electronic conductors (MIECs) are concentrated as good cathode candidates because their cathode kinetic reaction is improved by replacing the triple-phase-boundary (TPB) zone (electrolyte-cathode-air) with a double interphase (cathode-air) at intermediate temperature [3]. Previously, a new family of oxides with K_2NiF_4 structure has been reported as a good mixed ionic electronic conductor (MIEC) material [4–16]. The ideal K_2NiF_4 structure can be regarded as the alternative stacking of perovskite type layers and rock salt type layers. These materials can accommodate a significant amount of oxygen non-stoichiometry, due to their unique crystal structure characteristics. Generally, it's noted that oxygen ionic conduction in K_2NiF_4-type compounds may occur through a vacancy mechanism in the perovskite layers or through diffusion of interstitial oxygen in the rock-salt layers, whereas the electronic conduction behaviour comes from the *p*-type electronic conductivity in the perovskite layers [17–20]. Compared to the commonly used perovskite-type cathodes, K_2NiF_4-type structural materials have better thermal stability, smaller thermal expansion coefficients ($10.5–14.2 \times 10^{-6}$ K^{-1}) [21–23] which match better with those of the commonly used electrolytes, such as YSZ, $Ce_{0.9}Gd_{0.1}O_{2-\delta}$ (CGO) or $La_{0.9}Sr_{0.1}Ga_{0.8}Mg_{0.2}O_{3-\delta}$ (LSGM). Moreover, it's also found that these compounds display relatively high oxygen diffusion and surface exchange coefficients, which are two vital factors for cathode performance [24,25]. Owing to the above-mentioned favourable properties, K_2NiF_4-type structure of A_2BO_4 materials can be the promising candidates of cathode for IT-SOFCs.

The most extensively studied systems for such applications are Ln_2NiO_4 (Ln = La, Pr, Nd) [26–28]. However, there are scarce researchers in the SOFC field focused on the Ln_2CoO_4 oxides. Wang and Nie reported that $Ln_{2-x}Sr_xCoO_4$ (Ln = Pr and Sm)-based oxides could be applied as promising cathodes for SOFCs via studying their thermal stability and conduction properties. They also suggested that single K_2NiF_4-type structure phases could not be obtained, whereas it could be for $0.8 \leq x \leq 1.5$ [23,29,30]. C. Tealdi and the coworkers studied the transport properties of the $La_{2-x}Sr_xCoO_4$ solid solution and found $La_{0.8}Sr_{1.2}CoO_4$ has the maximum electrical conductivity in the whole temperature range (30–750 °C) [31]. Jin and Liu also studied the composition of $Ba_{1.2}Sr_{0.8}CoO_4$–GDC composite cathodes and results showed that the performance of composite cathode was enhanced greatly [32]. In our group, we adopted the same structure and also found $LaSrCoO_4$ and H–$LaSrCoO_4$ possess better electrochemical properties [33,34].

In the work described in this paper, composites containing gadolinia doped ceria (CGO) and $La_{0.8}Sr_{1.2}CoO_{4+\delta}$ (LSCO4) K_2NiF_4-type structure oxide were investigated. These combine the high oxygen-ion conductivity of CGO [35] and high electronic conductivity and fast oxygen surface exchange of LSCO4. The feasibility of LSCO4–CGO composites as cathode on LSGM electrolyte has been assessed in detail.

2. Experimental

2.1. Preparation of powders

The original material of $La_{0.8}Sr_{1.2}CoO_{4+\delta}$ (LSCO4) was prepared with a citric–nitrate process using stoichiometric quantities of $La(NO_3)_3 \cdot 6H_2O$, $Sr(NO_3)_2$, and $Co(NO_3)_3 \cdot 6H_2O$ (all in analytical purity) and in a citric acid to total metallic ions molar ratio of 4.5:1. A porous xerogel was formed at 110 °C and then transformed into

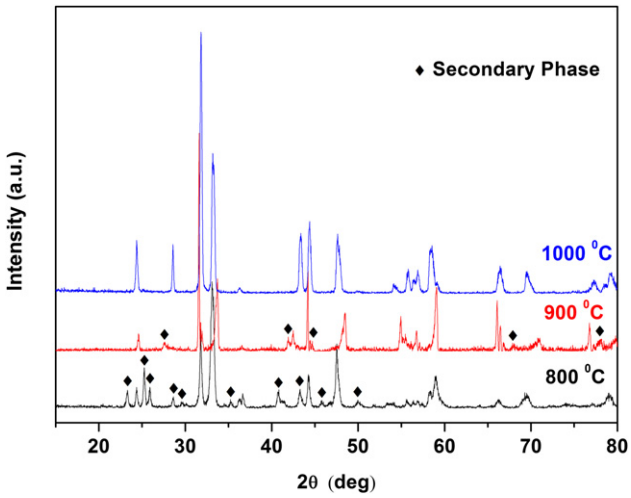

Fig. 1. XRD patterns of LSCO4 samples prepared at different temperatures.

LSCO4 black power after calcined at 1000 °C for 4 h in air. Similarly, stoichiometry amounts of $Ce(NO_3)_3 \cdot 6H_2O$ and Gd_2O_3 were dissolved in nitric acid and 4.5 mol citric acid was added per mole of nitrate. The mixtures were heated at 110 °C and then calcined at 700 °C for 2 h to remove residual organic matter and to ensure a single-phase composition of CGO. The mixture of the calcined LSCO4 and CGO powders was ground with acetone for 1 h for form composites with 15, 25, 35, and 45 wt % CGO (marked as LSCO4–15% CGO, LSCO4–25% CGO, LSCO4–35% CGO, and LSCO4–45% CGO, respectively).

The electrolyte $La_{0.9}Sr_{0.1}Ga_{0.8}Mg_{0.2}O_{3-\delta}$ (LSGM) was prepared by solid-state reaction. La_2O_3, $SrCO_3$, Ga_2O_3, and MgO were mixed after drying to remove the absorbed water. The mixture was ball-milled 1 h in the presence of acetone. Then, the mixture was pressed into a pellet and finally fired at 1500 °C for 10 h in air. A single perovskite phase was formed according to the XRD pattern. Pellets with thickness of 1.2 mm were prepared for electrolyte-supported cell tests.

Three-electrode half cells were fabricated as follows: mixed slurry was made of LSCO4–CGO and LSGM (in a weight ratio of 7:3) with organic additive containing terpilenol and turpentine. The mixture was then screen-printed onto one side of the LSGM electrolyte followed by calcination at 1000 °C for 3 h. A platinum

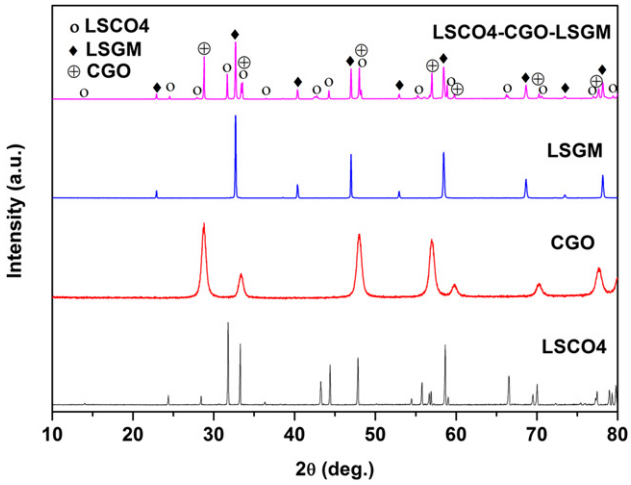

Fig. 2. XRD patterns of pre-synthesized LSCO4, CGO, LSGM, and LSCO4–CGO–LSGM mixture calcined at 1000 °C.

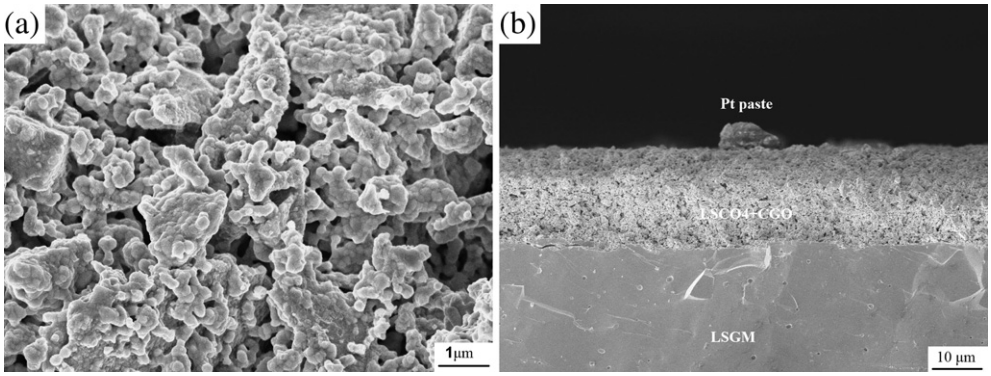

Fig. 3. SEM images of LSCO4–35% CGO composite cathode on LSGM electrolyte sintered at 1000 °C (a) surface view and (b) cross-section view.

counter electrode was laid symmetrically to the working electrode on the other side and another Pt reference electrode was placed at the edge of the electrolyte on the working electrode side. All the three electrodes were covered with Pt paste as current collector and treated at 900 °C.

The single cell was fabricated on a LSGM pellet with about 1.2 mm thickness. A layer of LSCO4–CGO composite cathode was first printed on one side of the LSGM pellet and fired at 1000 °C for 1 h. NiO-LSGM ink was then printed on the other side of the LSGM pellet and fired at 1000 °C for 1 h. The LSCO4–CGO composite cathode with an area of 0.48 cm^2 was about 35 μm thick after firing. Pt wire and Pt paste was used as current collectors for both electrodes and the cells were tested in a four-probe configuration.

2.2. Characterization

The reaction product was characterized by X-ray diffraction (XRD) for phase identification and to assess phase purity. The characterization was performed with powder X-ray diffraction (D/Max-2400, Rigaku, Japan) employing Cu Kα radiation at a step of 0.02° in a 2θ range of 10°–80°. The microstructure of the LSCO4–CGO composite cathode was inspected with JEOL JSM-6390 SEM. The polarization resistance (R_p) of the cathode/electrolyte interface as a function of temperature was determined by *AC* impedance spectroscopy employing the Solartron 1287 Electrochemical interface and 1260 Impedance/Gain-Phase analyzer over a frequency range of 10^{-2}–10^6 Hz under an applied amplitude of 10 mV. The *DC* polarization experiments were taken at various potential steps by recording the current density as a function of time. The cathode overpotential was calculated according to the following equation: $\eta_{WE} = \triangle U_{WR} - iR_{el}$, where $\triangle U_{WR}$ is the applied voltage between the working and reference electrodes, i is the *DC* current flowing through the cell and R_{el} is the electrolyte resistance derived from the impedance spectrum.

3. Results and discussion

3.1. Structure characterization

The XRD patterns of LSCO4 powders were sintered at different temperatures for 4 h are shown in Fig. 1. It's found that K_2NiF_4-type structure is not formed when calcination temperature is lower than 1000 °C. On the other side, for the effective application, the reaction between the electrolyte and electrode is undesirable for the long term stability of a SOFC. Therefore, the reactivity of LSCO4 with the LSGM electrolyte was further studied by mixing LSCO4, CGO, and LSGM powders with a 1:1:1 weight ratio, and sintered at 1000 °C for 10 h. Fig. 2 shows the XRD patterns of LSCO4, CGO, LSGM, and the LSCO4–CGO–LSGM mixture. It clearly exhibits that the main peaks of LSCO4, CGO, and LSGM were present and no other by-product phases were occurred, indicating that LSCO4 is chemical compatibility with CGO and LSGM.

3.2. SEM images

To investigate the microstructure of the composite cathode, SEM images were taken from both surface and cross-section. Fig. 3 exhibits the FESEM images of the LSCO4–35% CGO composite cathode on the LSGM electrolyte sintered at 1000 °C for 3 h. Fig. 3(a) shows that the particles are connected with each other, with an average grain size of about 2–3 μm. Meanwhile, the cathode displays a well-boned porous network, which is convenient for the oxygen transporting to the activated the three-phase boundary (TPB) sites. Fig. 3(b) gives the cross-section view of a fractured cell. The thickness of the composite cathode layer was approximately 30 μm. The attachment of the composite cathode is high and no delamination is observed at the LSCO4-35% CGO/LSGM interface.

3.3. Electrochemical performance

Electrochemical impedance measurements for LSCO4–CGO composite cathodes on LSGM electrolyte were performed at different temperatures without applying a bias voltage in air, as shown in Fig. 4. The associated electrical equivalent circuit is also exhibited in the inset of Fig. 4, and the fitting results are presented in Table 1. A high-frequency inductive component (L) coming from

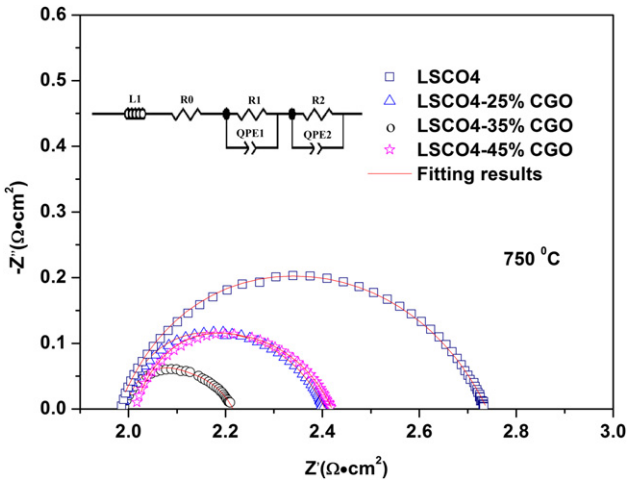

Fig. 4. Impedance spectra of LSCO4 and LSCO4–CGO composite cathodes on LSGM electrolyte at 750 °C under open-circuit-potential conditions.

Table 1
Polarization resistance of LSCO4–CGO composite cathodes on LSGM electrolyte at 750 °C.

Parameters	L (H cm^2)	R_s (Ω cm^2)	R_1 (Ω cm^2)	Q_1 (Ω cm^2 s^{-n})	R_2 (Ω cm^2)	Q_2 (Ω cm^2 s^{-n})	R_p (Ω cm^2)
LSCO4	1.63×10^{-6}	1.98	0.54	0.0026	0.21	0.0836	0.75
LSCO4–25% CGO	1.75×10^{-6}	2.13	0.23	0.0051	0.19	0.0146	0.42
LSCO4–35% CGO	1.77×10^{-6}	1.96	0.11	0.0015	0.10	0.0207	0.21
LSCO4–45% CGO	1.84×10^{-6}	2.11	0.29	0.0013	0.14	0.0101	0.43

the measuring system is visible at temperature above 650 °C; the series resistance, R_0, corresponds to the overall ohmic resistance from the electrolyte, electrodes and the connection wires; *QPE* is the constant phase element, R_1 and R_2 correspond to the high- and low-frequency arcs, respectively [36]. The high-frequency arc (R_1) reflects the charge transfer of oxygen ions at the electrode/electrolyte interface [37]. The low-frequency arc (R_2) corresponds to the oxygen adsorption or dissociation process [38]. The total polarization resistance (R_p) is the sum of R_1 and R_2.

From the impedance spectra, it can be seen that the R_p of pure LSCO4 and LSCO4–CGO composite cathodes change from 0.75 Ω cm^2 for LSCO4 to 0.21 Ω cm^2 for LSCO4–35% CGO at 750 °C. The 70% decrease of R_p contributes to the large oxygen vacancy in CGO which is beneficial to establish sufficient TPBs and increase the paths to transfer the oxygen ions. The R_p of LSCO4–35% CGO is much less than LaSrCoO4–BZCY composite cathode at the same temperature [32]. Here, BZCY shows a proton conductor. Though the difference of transfer mechanism between LSCO4–BZCY and LSCO4–CGO needs to be investigated, the lower R_p indicates that LSCO4 favours the oxygen ions rather than proton at some content. According to the fitting data in Table 1, compared with pure LSCO4 cathode, both R_1 and R_2 of LSCO4–35 wt % CGO composite cathode are much smaller, resulting the great difference of R_p values of two samples. This phenomenon can be explained as follows. As one kind of mixed ionic-electronic conductor, LSCO4 with K_2NiF_4-type structure, the oxygen reduction occurs not only on the TPB but also on the surface of electrode. As we known, the key to enable such intermediate temperature range of operation is to accelerate the oxygen reduction reaction in the cathode and the oxygen transport in the cathode and electrolyte. Generally, the overall reactions involving oxygen are:

$$\frac{1}{2}O_{2(g)} + 2e^-_{(\text{cathode})} \leftrightarrow O^{2-}_{(\text{cathode surface})} \quad (1)$$

$$O^{2-}_{(\text{cathode surface})} \leftrightarrow O^{2-}_{(\text{cathode bulk})} \quad (2)$$

$$O^{2-}_{(\text{cathode bulk})} \leftrightarrow O^{2-}_{(\text{electrolyte})} \quad (3)$$

The first reaction represents the reduction of oxygen on the cathode surface, the second reaction stands for the diffusion of oxygen into the cathode, the third reaction represents transfer of oxygen from the cathode to the electrolyte in which the oxygen ion proceeds to diffuse. Meanwhile, Adler et al. [38,39] demonstrated that the oxygen reduction reaction in MIEC electrodes is governed by the oxygen surface exchange and the oxygen diffusion. Therefore, the oxygen vacancy is important for the oxygen reduction reaction in SOFCs as they are likely to couple strongly to oxygen dissociation, transportation, and incorporation. Moreover, the diffusion is influenced by the concentration of oxygen vacancies [40]. Fig. 5 depicts the possible process of oxygen reduction reaction in LSCO4–CGO composite cathode on LSGM electrolyte. The addition of CGO with proper content in LSCO4 gives more channels to transport oxygen ions via increasing the concentration of total oxygen vacancies. Simultaneously, the TPB increases when CGO is added into $La_{0.8}Sr_{1.2}CoO_4$ as a composite cathode. Thus, the ORR can occur at much more TPB, then, more oxygen ions may diffuse to the LSGM electrolyte, and oxygen diffusion is enhanced. After adding 35 wt % CGO in LSCO4, the reduction of R_1 clearly shows that the charge-transfer process for oxygen reduction on the porous composite cathode was improved at the TPB.

The area specific resistances (ASRs) values for the composite cathodes at different temperatures are exhibited in Fig. 6. These show strong dependence relative contents of CGO and LSCO4, with the lowest ASR value being observed from the specimen of LSCO4–35% CGO. At values larger than 35 wt % of CGO in LSCO4, the ASR increases as it is related to the effective percolation of electrically conducting phase present [41]. ASR will also be seemed to rise obviously at lower content of CGO, as there is significant detrimental effect due to reduced TPB. Arrhenius plots of the ASRs

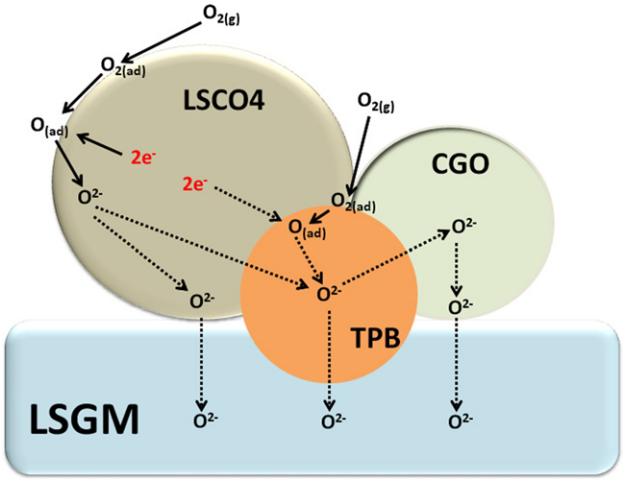

Fig. 5. Schematic of the possible process of oxygen reduction reaction in LSCO4–CGO composite cathode.

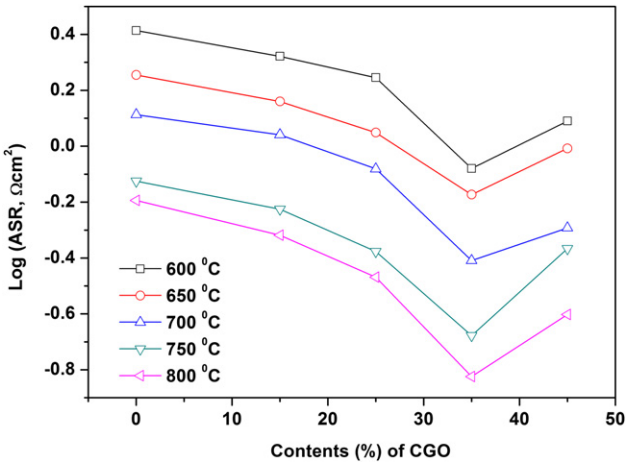

Fig. 6. Dependence of cathodic polarization upon content of CGO at different temperatures.

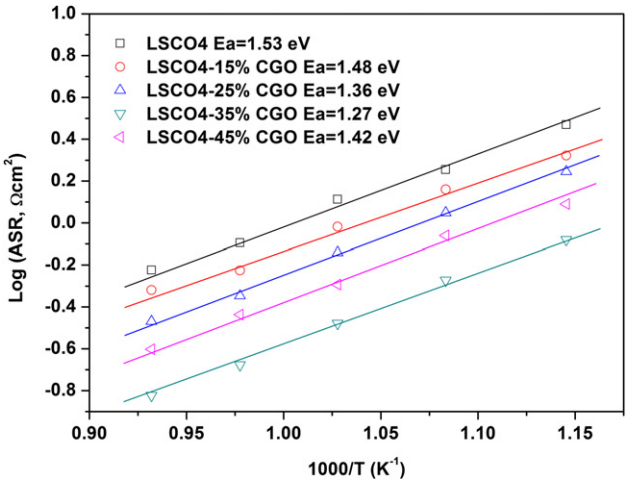

Fig. 7. Arrhenius plot of the area specific resistance results for various composite cathodes of CGO with LSCO4 onto LSGM electrolyte.

are also marked in Fig. 7. Activation energies were calculated using Eq. (4).

$$\log R_P = \log R_0 - \frac{E_a}{2.303RT} \quad (4)$$

where, R is a universal gas constant, T is absolute temperature, and R_0 is related to the pre-exponential term in Eq. (4). Generally, the E_a in the exponential term is activation energy, which is directly related to the slop of Fig. 7 and originates from all of the cathode processes including oxygen adsorption, dissociation, bulk or surface diffusion, and the self-diffusion via electrolyte [41]. For comparison, the activation energy of $LaSrCoO_4$ with BZCY composite cathode was reported as 1.40 eV [32] and the value for LSCO4–CGO composite cathodes (except LSCO4–15% CGO) are significantly lower, indicating that the oxygen reduction process LSCO4–CGO composite cathodes are faster and have a lower temperature dependence than $LaSrCoO_4$ with BZCY composite cathode. Generally, the concept of composite cathode is used in order to maximize the TPB between cathode and electrolyte to enhance performance [41]. In addition, the enhanced cathode performance of LSCO4–35% CGO is not only the effect of maximized

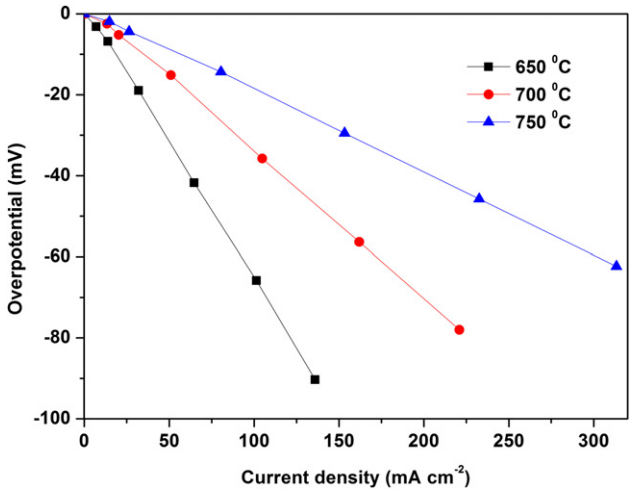

Fig. 8. Overpotential-current density curves of the LSCO4–35% CGO composite cathode.

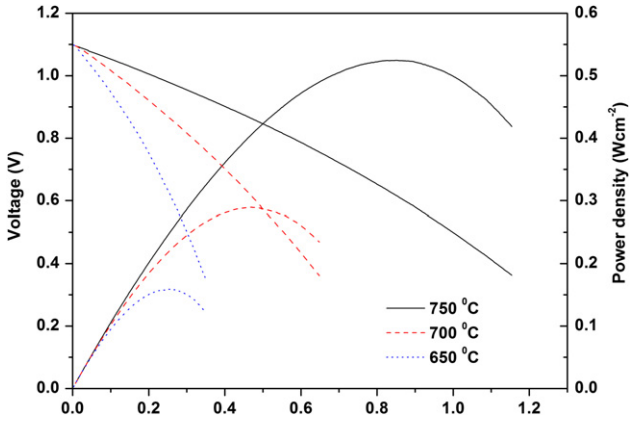

Fig. 9. Cell voltages and power densities as function of current density of LSGM-supporting cell with LSCO4–35% CGO cathode, NiO as anode, and measured in humidified H_2 and air in temperature range of 650–750 °C.

composite cathode but also property of MIEC caused by various easy oxygen pathways as one of the properties in layered perovskite [42]. The activation energy of LSCO4 is 1.53 eV in Fig. 7. The composite cathodes, for example, from LSCO4–25% CGO to LSCO4–45% CGO, exhibit activation value decreasing to 1.27 eV because of the extension of chemically active sites as the TPB expands giving an enhanced oxygen reduction process in the composite cathode.

Cathodic overpotential, defined as the deviation from reversible potential as electric current passes via a cathode, is attributed to the slowness of ORR and is an important factor representing the electrode performance. The cathodic polarization curves for LSCO4–35% CGO composite materials are exhibited in Fig. 8. As can be seen, the lowest polarization overpotential of 63 mV is measured for a LSCO4–35% CGO composite cathode at current density of 313 mA cm^{-2} at 750 °C. Moreover, at the whole tested range, there appears a linear relationship [43], $i = i_0ZF\eta/RT$, where i is the current density, i_0 is the exchange-current density, η is the overpotential, F is the Faraday constant and R is the universal gas constant. From the inverse of the derivative of i against η, the polarization resistance can be calculated. The value obtained at 750 °C is 0.20 Ω cm^2, which is quite agreement with the result obtained from the impedance measurement.

We applied the LSCO4–35% CGO composite cathode to a LSGM electrolyte-supporting SOFC with NiO anode. The curves of cell voltage and the corresponding power density versus current density are exhibited in Fig. 9. The OCVs are quite close to the values of Nernst potential expected when using humidified H_2 as a fuel and demonstrate the cells are well-sealed with gastight electrolytes [44]. The cell shows proper performances with maximum output power densities of 515 mW cm^{-2} at 750 °C. The encouraging performances reinforce the advantages of a composite cathode system to attain maximum cell performance in this system.

4. Conclusions

In summary, LSCO4 powders with K_2NiF_4-type structure were prepared by citric-nitrate method and characterized by XRD and SEM. Incorporating an amount of $Ce_{0.9}Gd_{0.1}O_{2-\delta}$ is to obtain a series of composite cathode LSCO4–CGO. Then the composite materials were studied in comparison with pure LSCO4 on electrochemical properties, such as the polarization curves and the electrochemical impedance spectra. The best electrochemical performance in symmetrical half cells was seen in the specimens that comprised a composite of 65 wt % LSCO4 and 35 wt % CGO (LSCO4–35% CGO).

This composite exhibited half cell ASRs of 0.21 Ω cm^2 and cell power density of 515 mW cm^{-2} at 750 °C, respectively. All of these results imply that that the LSCO4 and CGO composite is a proper promising cathode material for IT-SOFCs applications.

References

[1] N.P. Brandon, S. Skinner, B.C.H. Steel, Rev. Mater. Sci. 33 (2003) 183.
[2] C. Xia, M.L. Liu, Adv. Mater. 14 (2002) 521.
[3] S.D. Park, J.M. Vohs, R.J. Gorte, Nature (London) 404 (2000) 265.
[4] A. Aguadero, J.A. Alonso, M.J. Escudero, L. Daza, Solid State Ionics 179 (2008) 393–400.
[5] Q. Li, H. Zhao, L.H. Huo, L.P. Sun, X.L. Cheng, J.C. Grenier, Electrochem. Commun. 9 (2007) 1508–1512.
[6] F. Zhao, X.F. Wang, Z.Y. Wang, R.R. Peng, C.R. Xia, Solid State Ionics 179 (2008) 1450–1453.
[7] J.B. Huang, R.F. Gao, Z.Q. Mao, J.Y. Feng, Int. J. Hydrogen Energy 35 (2010) 2657–2662.
[8] Y.F. Wang, J.G. Cheng, Q.M. Jiang, J.F. Yang, J.F. Gao, J. Power Sources 196 (2011) 3104–3108.
[9] C. Jin, J. Liu, Y.H. Zhang, J. Sui, W.M. Guo, J. Power Sources 182 (2008) 482–488.
[10] J.M. Bassat, P. Odier, A. Villesuzanne, C. Marin, M. Pouchard, Solid State Ionics 167 (3–4) (2004) 341–347.
[11] A.J. Jennings, S.J. Skinner, Solid State Ionics 152–153 (2000) 663–667.
[12] T. Omata, K. Ueda, N. Ueda, M. Katada, S. Fujitsu, T. Hashimoto, H. Kawazoe, Solid State Commun. 88 (1993) 807.
[13] V. Vashook, S.P. Tolochko, I.I. Yushkevich, L.V. Makhnach, I.F. Kononyuk, H. Altenburg, J. Hauck, H. Ullrnann, Solid State Ionics 110 (1998) 245–253.
[14] K. Ishikawa, S. Kondo, H. Okanc, S. Suzuki, Y. Suzuki, Bull. Chem. Soc. Jpn. 60 (1987) 1295–1298.
[15] Y. Cao, H. Gu, H. Chen, Y. Zheng, M. Zhou, L. Guo, Int. J. Hydrogen Energy 35 (2010) 5594–5600.
[16] Y. Yin, B. Liu, J. Qi, Y. Gu, Q. Liao, Z. Qin, Z. Li, Q. Wang, Y. Zhang, J. Power Sources 196 (2011) 6238–6241.
[17] V.V. Kharton, A.A. Yaremchenko, A.L. Shaula, M.V. Patrakeev, E.N. Naumovich, D.I. Logvinovich, J.R. Frade, F.M.B. Marques, J. Power Sources 177 (2004) 26–37.
[18] T. Shimura, K. Suzuki, H. Iwahara, Solid State Ionics 104 (1997) 79–88.
[19] A. Tarancon, M. Burriel, J. Santiso, S.J. Skinner, J.A. Kilner, J. Mater. Chem. 20 (2010) 3799.
[20] S.J. Skinner, J.A. Kilner, Solid State Ionics 135 (2000) 709–712.
[21] M.A. Daroukh, V.V. Vashook, H. Ullmann, F. Tietzb, I. Arual Raj, Solid State Ionics 158 (2003) 141–150.
[22] A.M. Hernández, J.V. Castillo, L. Mogni, A. Caneiro, Int. J. Hydrogen Energy 36 (2011) 15704–15714.
[23] Y.S. Wang, H.W. Nie, S.R. Wang, T.L. Wen, U. Guth, V. Valshook, Mater. Lett. 60 (2006) 1174–1178.
[24] E. Boehm, J.M. Bassat, M.C. Steil, P. Dordor, F. Mauvy, J.C. Grenier, Solid State Sci. 5 (2003) 973–981.
[25] E. Boehm, J.M. Bassat, P. Dordor, F. Mauvy, J.C. Grenier, Ph. Stevens, Solid State Ionics 176 (2005) 2717–2725.
[26] A. Chroneos, D. Parfitt, J.A. Kilner, R.W. Grimes, J. Mater. Chem. 20 (2010) 266.
[27] C. Lalanne, F. Mauvy, J.M. Bassat, J.C. Grenier, P. Dordor, P. Stevens, in: M. Mogensen (Ed.), Proceedings of the Sixth European SOFC (2004), ISBN 3-905592-15-0, pp. 1351–1359.
[28] D. Pérez-Coll, A. Aguadero, Fuel Cells 11 (2011) 91–101.
[29] H.W. Nie, T.L. Wen, S.R. Wang, Y.S. Wang, U. Guth, V. Vashook, Solid State Ionics 177 (2006) 1929–1932.
[30] C.N. Munnings, S.J. Skinner, G. Amow, P.S. Whitfield, I.J. Davidson, Solid State Ionics 176 (2005) 1895–1901.
[31] C. Tealdi, C.L. Malavasi, P. Mustarelli, C. Ritter, G. Chiodelli, Y.A. Diaz-Fernandez, Phys. Rev. B 82 (2010) 174118.
[32] C. Jin, J. Liu, J. Alloys Compd. 474 (2009) 573–577.
[33] B. Peng, G. Chen, T. Wang, J. Zhou, J. Guo, Y.H. Cheng, K. Wu, J. Power Sources 201 (2012) 174–178.
[34] J. Zhou, G. Chen, K. Wu, Y.H. Cheng, B. Peng, J. Guo, Y.Z. Jiang, Appl. Surf. Sci. 258 (2012) 3133–3138.
[35] B.C.H. Steele, J. Solid State Ionics 129 (2000) 95.
[36] V.V. Vashook, J. Zoel, T.L. Wen, U. Guth, Solid State Ionics 177 (2006) 1827.
[37] C.J. Fu, K.N. Sun, N.Q. Zhang, X.B. Chen, D.R. Zhou, Electrochim. Acta 52 (2007) 4589–4594.
[38] S.B. Adler, Solid State Ionics 111 (1998) 125–134.
[39] S.B. Adler, J.A. Lane, B.C.H. Steele, J. Electrochem. Soc. 143 (1996) 3554.
[40] S. Li, Z. Lu, B. Wei, X. Huang, J. Miao, Z. Liu, W. Su, J. Alloys Compd. 448 (2008) 116–121.
[41] A. Barbucci, M. Viviani, M. Panizza, M. Delucchi, G.J. Cerisola, Appl. Electrochem. 35 (2005) 399.
[42] G. Kim, S. Wnag, A.J. Jacobson, L. Reimus, P. Brodersen, C.A. Mims, J. Mater. Chem. 17 (2007) 2500.
[43] B.C.H. Steele, Solid State Ionics 75 (1995) 157–165.
[44] B. Wei, Z. Lu, S. Li, Y. Li, K. Liu, W. Su, Electrochem. Solid-State Lett. 8 (2005) A428.